

Positronium cooling in porous silica measured via Doppler spectroscopyD. B. Cassidy,¹ P. Crivelli,² T. H. Hisakado,¹ L. Liskay,^{3,*} V. E. Meligne,¹ P. Perez,³ H. W. K. Tom,¹ and A. P. Mills Jr.¹¹*Department of Physics and Astronomy, University of California, Riverside, California 92521-0413, USA*²*URFJ, Rio de Janeiro, Brazil*³*CEA, Saclay, IRFU, F-91191 Gif-sur-Yvette Cedex, France*

(Received 10 November 2009; published 29 January 2010; corrected 2 March 2010)

We have measured the kinetic energy of positronium (Ps) atoms emitted into a vacuum from a porous silica film subsequent to positron bombardment, via the Doppler spread of the linewidth of the Ps 1^3S-2^3P transition. We find that the deeper in the target film that positrons are implanted the colder is the emitted Ps, an effect we attribute to cooling via collisions in the pores as the atoms diffuse back to the film surface. We observed a lower limit to the mean Ps kinetic energy associated with motion in the direction of the laser, $E_x = 42 \pm 3$ meV, that is consistent with conversion of the confinement energy of Ps in the 2.7-nm-diameter pores to kinetic energy in vacuum. An implication is that a porous sample would need to be composed of pores greater than around 10 nm in diameter in order to produce thermal Ps in vacuum with temperatures of less than 100 K. By performing Doppler spectroscopy on intense pulses of Ps we have experimentally demonstrated the production of many excited-state Ps atoms simultaneously, which could have numerous applications, including laser cooling and fundamental spectroscopic studies of Ps and the production of antihydrogen.

DOI: [10.1103/PhysRevA.81.012715](https://doi.org/10.1103/PhysRevA.81.012715)

PACS number(s): 34.80.Lx, 36.10.Dr, 78.70.Bj

I. INTRODUCTION

Positronium (Ps), the metastable electron-positron bound state [1], may be produced with high efficiency by implanting a low-energy positron beam into an appropriate target [2]: if a metal is used Ps may be created at the surface [3,4] but not in the bulk material, since screening by the conduction electrons prevents Ps binding [5]. If an insulator is used Ps can be formed in the bulk material [6] or at the surface [7].

In recent years considerable attention has been given to the production of Ps in various porous insulators or semiconductors [8] in view of their potential importance to microelectronics [9], catalysts [10], and many other applications. Positronium produced in this kind of target is mostly created in the bulk material, from where it may diffuse to the internal pores. Once in a void Ps can live for a significant fraction of the vacuum lifetime, depending on the pore size [11–13]. In general such Ps atoms will lose energy via collisions with the internal pore surfaces, become trapped in the pores, and cool down to near thermal energies.

The details of the pore structure can strongly affect the subsequent behavior of Ps created in this way. If the pores are isolated then the Ps will simply be localized within them. If they are interconnected Ps will diffuse between different pores and if the interconnects extend to the target surface Ps may be emitted into vacuum. Moreover, it is possible to produce well-defined pore structures, such as aligned channels in one or two dimensions or three-dimensional arrays [14], the nature of which can also play a role in positronium characteristics.

Such materials are well suited to the study of fundamental interactions between Ps atoms [15] since a porous structure may act essentially as a trap and increase the likelihood of more than one atom being in the same void at the same time, if the instantaneous positron beam density is high enough.

Implanting intense positron pulses into porous silica films has made it possible to observe the spin exchange quenching of long-lived triplet Ps states [16] and the formation of molecular Ps [17]. Extending these methods is expected to lead to the production of higher Ps densities, with the eventual goal of producing a Bose-Einstein condensate [18]. A critical aspect of this work is the production of low-temperature Ps, which is necessary to facilitate the phase transition from a thermal cloud to the condensed state.

Another area in which cold Ps may prove useful is the production of antihydrogen [19] by the charge exchange reaction of positronium with antiprotons [20–22]. Some experimental schemes in this area [23,24] call for clouds of excited-state Ps atoms that interact with antiprotons to produce antihydrogen. A promising way to achieve this would be to laser excite cold ground-state Ps atoms [25] emitted into the vacuum from porous films.

The experiments we report here involve producing Ps in porous silica films using intense positron pulses. The structure of the films is such that some of the Ps created in the pores is emitted into vacuum, where it is excited to the $2P$ state using a pulsed laser tunable around the Ps Lyman α wavelength at 243 nm. The experiment was conducted in an axial magnetic field of 700 G and consequently Zeeman mixing of (some) excited triplet P states with singlet states increased the overall Ps decay rate. Thus, we were able to observe the 1^3S-2^3P excitation of Ps via changes in lifetime spectra that were correlated with the laser pulses. By making such measurements for different laser frequencies we could then observe the Doppler broadening of this transition and hence measure the Ps temperature in the direction of the laser.

II. EXPERIMENTAL PROCEDURE**A. Positronium production and observation**

The experiments were carried out using a positron accumulator that has been described elsewhere [26]. This system

*On leave from KFKI Research Institute for Nuclear and Particle Physics, P.O. Box 49, H-1525 Budapest, Hungary.

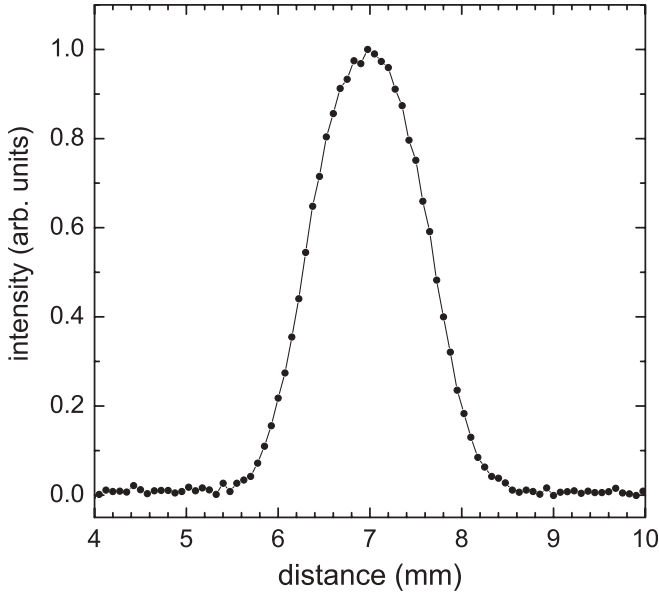


FIG. 1. Positron beam profile measured using a phosphor screen. The size of the beam was set by applying 6 MHz to the rotating wall electric field in the accumulator and was chosen to facilitate overlap with the primary and reflected laser beams.

uses a two-stage Surko trap [27] to supply positron pulses to an accumulator wherein plasmas containing up to 1×10^8 particles may be generated and whose density may be adjusted by a “rotating wall” electric field [28,29]. These plasmas are ejected from the accumulator by an ~ 300 -V pulsed harmonic potential, which compresses them in time [30] to a width that depends in part on the space charge potential of the plasma. For the experiments described here plasmas containing around 2×10^7 positrons with a full width at half maximum (FWHM) of ~ 1.5 mm were used, and these typically had a time width of ~ 20 ns. The positron beam profile is shown in Fig. 1.

Upon ejection from the accumulator, positron plasmas were implanted into the Ps formation target, which was a thin silica film that is described in detail later in this article. The beam impact energy was controlled by a linear accelerator just in front of the target. The accelerator was a series of 11 annular electrodes interconnected by 1-M Ω resistors, across which the full accelerating potential (0–10 kV) was applied. The resulting modest potential gradient prevented beam distortion and did not affect the pulse timing.

Positronium created in the target was observed using the technique of single-shot positron annihilation lifetime spectroscopy (SSPALS) [31]. A 50-mm-diameter \times 40-mm-long lead tungstate (PbWO₄) scintillator attached to a Hamamatsu R2083 photomultiplier tube (PMT) was used [32] to detect annihilation radiation resulting from the initial positron impact and subsequent Ps decay. The center of the scintillator was located about 75 mm from the center of the Ps forming target. The output from the detector was connected directly to a 6-GHz bandwidth digital oscilloscope that was operated with a sampling rate of 20 GHz. The intrinsic time resolution of the detector was ~ 15 ns, owing to the decay time of the scintillator, which was more than adequate for the present measurements.

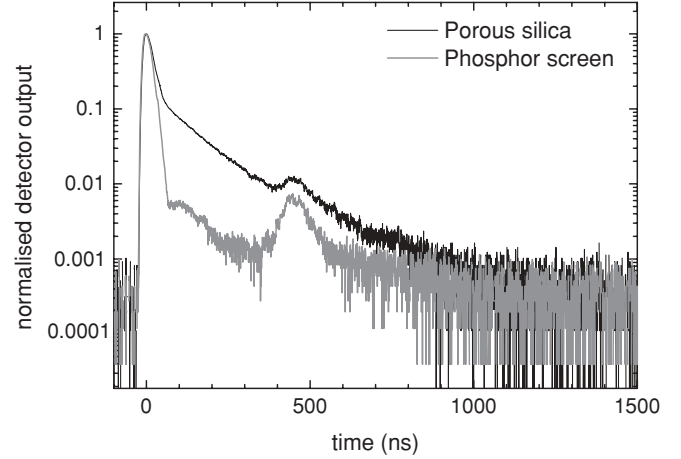


FIG. 2. Example of single-shot lifetime spectra taken with and without Ps formation. A 1.5-kV beam incident on a porous silica film produces $\sim 40\%$ Ps while a 5-kV beam implanted into a phosphor screen produces virtually no Ps. Several features present in both spectra are actually properties of the PMT (see [32] for details). In particular the bump starting at ~ 400 ns is due to ion feedback and because of this we generally truncate our spectra at $t < 300$ ns. The spectrum taken with the phosphor screen may be considered to be the system response.

An example of a single-shot lifetime spectrum is shown in Fig. 2. In principle such data may be decomposed and analyzed to provide the lifetime and intensity of all of the decay components that make up the spectrum [15]. For the present purposes, however, it is sufficient to compare the counts in the “prompt peak” with those at later times to obtain an approximation of the Ps formation fraction. We define the delayed fraction, f_d , as

$$f_d = \int_{50 \text{ ns}}^{300 \text{ ns}} V(t) dt \bigg/ \int_{-50 \text{ ns}}^{300 \text{ ns}} V(t) dt. \quad (1)$$

Here $V(t)$ is the detector output voltage, which is approximately proportional to dN/dt , where N is the number of annihilation γ rays. The delayed fraction thus defined is approximately related to the triplet Ps fraction f_3 (i.e., the fraction of incident positrons annihilating as triplet Ps) as $f_3 \approx f_d e^{t/\tau}$, where τ is the mean lifetime of the delayed Ps annihilation and $t = 50$ ns.

The emission of Ps into vacuum may be inferred from the ~ 130 -ns lifetime component seen in Fig. 2, which is consistent with the 135 ns computed from the average of the 128-ns lifetime for triplet $m = 0$ in a field of 0.07 T [33,34] and the 142-ns lifetime of triplet $|m| = 1$ Ps in vacuum, with equal weighting of the two components as dictated by the angular distribution of the 3γ annihilation photons [35]. No such component was seen in previous experiments in which similar target films were used that had nonporous capping layers on the surface to prevent Ps emission. The space between the Ps formation target and the front of the accelerator formed the effective interaction region between the laser beams and the Ps cloud.

The layout of the Ps-laser interaction region is shown schematically in Fig. 3. Light from an enclosed laser room is directed into the vacuum chamber through fused quartz

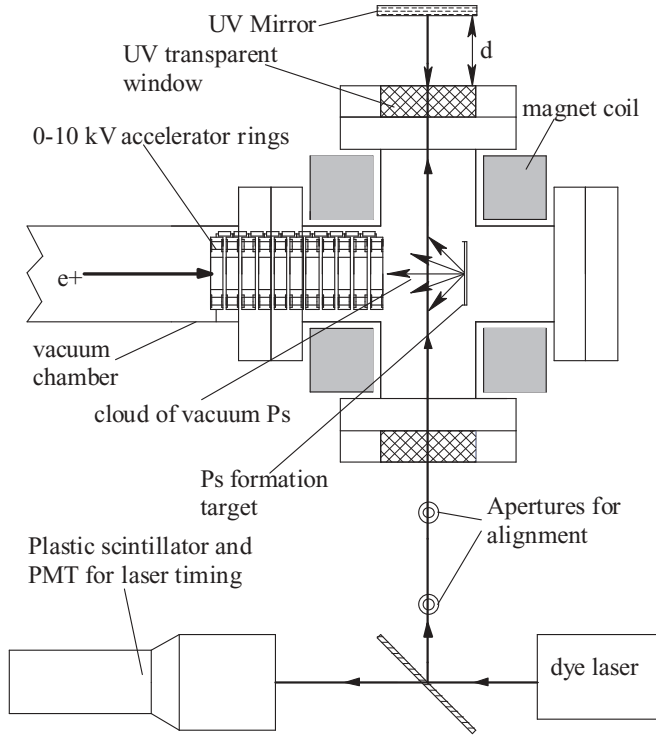
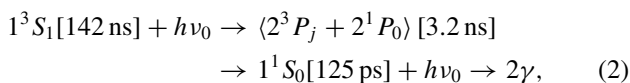


FIG. 3. Layout of the positronium-laser interaction region. The laser and positronium beams are not to scale. The laser was either directed into the target chamber or reflected to the plastic detector but not both simultaneously. The magnetic field in the target region is 700 G. When the beam was reflected back with minimal delay ($d = 5$ cm) the effective power of the beam was doubled with respect to the maximal delay ($d = 5$ m).

windows and is retro-reflected back into the interaction region to increase the effective laser power available. The laser light may be directed into a plastic scintillator that is also able to detect the γ -ray pulse following the positron dump, so that the relative timing between the two may be controlled. As explained further below, the distance d between the UV mirror and the vacuum chamber could be varied from a few cm to more than 5 m in order to provide either a single pulse (with nearly double the power) or two temporally separated pulses. Care was taken to avoid laser light directly irradiating the target as this can create both short- and long-lived paramagnetic centers that affect the formation and decay of Ps [36,37]. While it is possible that some light reflected in the vacuum chamber may have hit the film, no detectable changes in the Ps formation characteristics were observed that could be attributed to the presence of laser light.

The basis of our experimental signal is the fact that when excited to the 2^3P_j ($j = 0, 1, \text{ or } 2$) state in a magnetic field some Ps atoms will decay back to the singlet ground state, which has a much larger decay rate than the triplet state. That is, excitation at the resonant frequency ν_0 can lead to the following sequence of events (the relevant decay times are given in square brackets):



where $(2^3P_j + 2^1P_0)$ represents a mixture of the $2P$ singlet and triplet states and 2γ refers to the two 511-keV annihilation γ rays following the decay of the singlet ground state. Since this is the signal that we measure we would like to know what fraction of excited states will decay in this way. We note that magnetic quenching also occurs for ground-state Ps [11] but that much stronger fields are required to mix the ground-state triplet levels because the ground-state hyperfine interval is much larger than those of the $n = 2$ states.

Optical and static electric fields couple only to states of differing orbital angular momentum, whereas a static magnetic field couples only to the spin magnetic moments of the positron and electron. Irrespective of the presence of a static magnetic field, the relatively broad band laser excites the ground-state triplet positronium 1^3S_1 states to various sublevels of the three 2^3P_j states. The static magnetic field B couples the triplet $m = 0$ components of the latter set to the 2^1P_0 state with a strength $x = 2\mu B/h$. The pure Zeeman effect in the first excited state of positronium is known in detail [38–40]. To approximate the ensuing magnetic quenching effect we assume that the 2^3P_j levels are all degenerate and separated from the 2^1P_0 state by an effective energy $\Delta \approx 2.5$ GHz. The P states are not magnetically coupled to the S states and therefore decay only via optical transitions to the ground state at a common rate $\gamma = 3.2 \text{ ns}^{-1}$. Denoting the triplet $m = 0P$ state as $|t\rangle$ and the singlet P state as $|s\rangle$ the simplified Hamiltonian is then

$$\begin{aligned} H &= \left(\frac{1}{2}\Delta - \frac{i}{2}\gamma \right) |t\rangle\langle t| \\ &+ \left(-\frac{1}{2}\Delta - \frac{i}{2}\gamma \right) |s\rangle\langle s| + x(|t\rangle\langle s| + |s\rangle\langle t|). \end{aligned} \quad (3)$$

Assuming the P states start as pure triplet, the subsequent evolution of the state is

$$|\psi(t)\rangle = \exp\{-iHt/\hbar\} |t\rangle. \quad (4)$$

The fraction of the annihilations that proceed via 2γ 's from the ground singlet state is then

$$Q = \int_0^\infty \gamma dt |\langle s|\psi(t)\rangle|^2 \approx \frac{1}{2}x^2 \left[x^2 + \frac{1}{4}\Delta^2 \right]^{-1} \approx 0.37, \quad (5)$$

using the fact that $\gamma \ll \Delta$. Including the $m = \pm 1$ states, the fraction of all the excited P states that end up decaying via two photons from the singlet ground state is then $\frac{1}{3}Q \approx 0.12$. The actual signal observed will be somewhat larger given that our laser pulse is significantly longer than 3.2 ns so that multiple transitions are possible for a given atom.

B. Porous silica target

The porous silica films were prepared using the cationic surfactant cethyl trimethylammonium chloride (CTACI) as pore generator agent and tetraethoxysilane (TEOS) as the mineral source for the silica network skeleton. The sol-gel process used a pure aqueous evaporation-induced self-assembly (AEISA) method [41], with a CTACI/TEOS molar ratio of 0.22. The films were deposited on a 0.15-mm-thick standard borosilicate microscope cover glass using spin coating at 1000 rpm. The surfactant was removed by heating the films at 450°C in air for

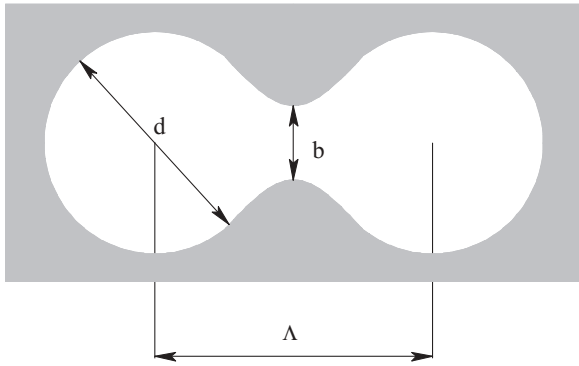


FIG. 4. A schematic representation of two interconnected pores in the target film. The nearly spherical pores have a diameter d and are connected to other pores via holes of diameter b . The separation between pores Λ is simply the pore diameter plus the wall thickness.

15 min. The sample was mounted in the vacuum chamber for positron measurements within a few minutes after the removal of the porogen.

The film thickness was more than 600 nm and the density $\rho \sim 1.35 \text{ g/cm}^3$. Positron lifetime measurements found 41% ortho-positronium reemission yield at 1-keV beam energy and 34% at 3 keV in a film grown with the same method [42]. A lifetime of $\sim 50 \text{ ns}$ in the pores was measured by capping the films.

The pore diameter is approximately 2.7 nm [41]. In contrast with Ref. [41], x-ray diffraction found no long-range order in the pore structure, although we would still expect the microscopic structure to consist of approximately spherical pores interconnected via short channels, as shown in Fig. 4. This figure shows a representation of only two spherical pores of diameter d connected by a hole of diameter b . If the porous films retain their hexagonal close packing (HCP) structure (at least over a short range) then we would expect each pore to have 12 nearest neighbors, all of them connected in a manner similar to that shown in the figure. Thus, with pores connected by channels of diameter b we expect, just from the geometry, the mean number of collisions per pore to be $C \approx d^2/3b^2$.

The spacing between pores, Λ , is the mean free path for Ps atoms that tunnel from pore to pore (which is discussed in more detail later in this article). This is given by the pore diameter plus the wall thickness and may be determined from the mean density of the porous material. For hollow spheres of diameter d and nearest neighbor distance Λ in a HCP arrangement within a material of density ρ_0 , the average density is approximately $\rho = (1 - \pi d^3/\Lambda^3 \sqrt{18})\rho_0$. Using $\rho/\rho_0 = 1.35 \text{ g cm}^{-3}/2.2 \text{ g cm}^{-3} = 0.61$ we obtain $\Lambda \approx 1.24d = 3.3 \text{ nm}$ [43].

C. Laser systems

The UV light used for the experiment was produced using a tunable Nd:YAG-pumped dye laser system that was capable of providing light over a range of $243 \pm 5 \text{ nm}$. All the lasers and most of the optics were contained in an especially constructed clean room adjacent to the positron beam. A Q -switched Nd:YAG laser (Continuum Surelite I-20) with second- and third-harmonic generators was used to provide

532- and 355-nm light pulses, respectively, with a 7-ns time duration (FWHM). This laser was pumped by flash lamps which were fired continuously at 20 Hz in order to keep the temperature of the YAG rod stable, but were Q -switched at lower repetition rate in coincidence with the positron beam as required. After separating the fundamental and two harmonic outputs, the 532-nm pulse was used to pump a Spectra Physics PDL-1 tunable dye laser using LDS 765 dye to produce 772-nm light. The tunable 772- and 355-nm (third harmonic of Nd:YAG) pulses were telescoped to the same spatial size and overlapped temporally and then frequency summed in a phase-matched β -barium borate (BBO) crystal to produce pulses of 243-nm light [44]. The dye laser was tuned simultaneously with the phase-matching angle of the BBO to produce tunable 243-nm pulses with energies of up to $350 \mu\text{J}$ per pulse.

The 243-nm wavelength was measured using $\sim 10\%$ of the total output in a SPEX 0.75 m Czerny Turner spectrometer with $10\text{-}\mu\text{m}$ entrance and exit slits using a 1200 lines/mm grating in fifth order. The spectrum was calibrated against the He-Ne laser line at 632.816 nm in second order from the diffraction grating. This arrangement had a resolution of 0.0015 nm and an absolute accuracy limited by the collinear alignment of the He-Ne and 243-nm laser beams which we were careful to align better than $20 \mu\text{rad}$ to limit misalignment errors to $\sim 0.005 \text{ nm}$. When the dye laser was operated using its grating in third order, the 243-nm linewidth was 0.002 nm and was 0.02 nm when the grating was used in first order. In the experiments reported here we used the 0.02-nm linewidth output in order to increase the signal to a useful level. The 243-nm beam was guided to the Ps formation chamber (see Fig. 3) using KrF (248 nm) dielectric mirrors and a pair of fused silica lenses. A schematic of the optical layout of this system is shown in Fig. 5. Note that all laser wavelengths are measured in air.

III. RESULTS

Single-shot lifetime spectra [31] were used to measure the formation of Ps in vacuum and to observe the interactions of resonant laser light with these atoms. The amount of triplet

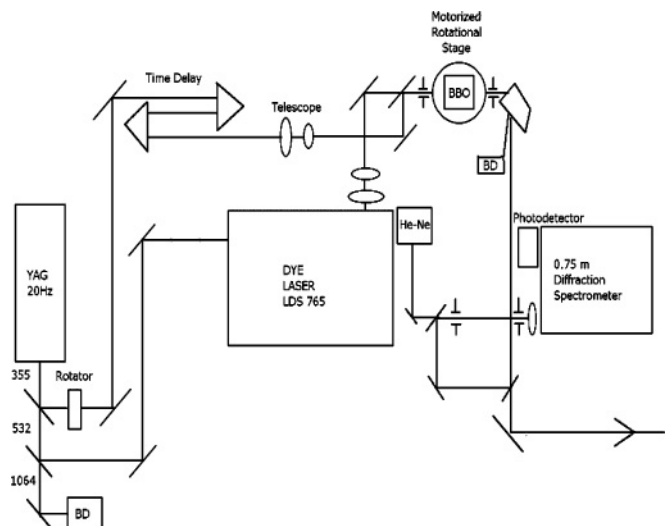


FIG. 5. Schematic of the optical layout of the laser system.

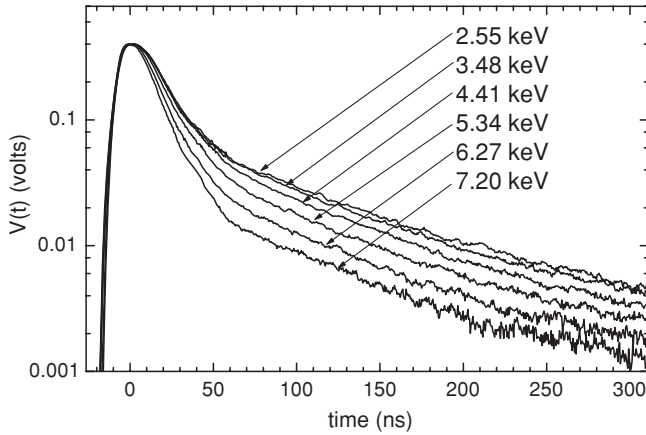


FIG. 6. Single-shot lifetime spectra for different positron beam energies, as indicated in the figure. Implanting the positron beam deeper into the sample reduces the amount of Ps that subsequently escapes into the vacuum. Note that in this and subsequent spectra $V(t)$ is given in volts. In fact the spectra have all been normalized to a peak height of 0.4 V. However, the individual peaks were all within $\sim 10\%$ of this value and $V(t)$ is a close approximation to the actual detector output voltage measured following a 9-dB 50 Ω attenuator.

Ps emitted into the vacuum varied with the incident positron beam energy, as may be seen in Fig. 6 [see also Eq. (1)]. At higher energies positrons are implanted deeper into the sample, and it is therefore more likely that positronium will annihilate via interactions with the walls before diffusing out into the vacuum. By the same token, increased interaction with the walls also means that the mean temperature of emitted Ps atoms will decrease with increasing beam energy, as discussed later.

When the laser is fired tuned to the Ps 1^3S-2^3P resonance, lifetime spectra such as those shown in Fig. 6 are perturbed by a pulse of increased annihilation rate due to the resonantly excited $2P$ states that are Zeeman mixed with short-lived singlet states. This increase in the annihilation rate is shown in Fig. 7, along with laser pulses that were measured separately using a plastic scintillator. Two laser pulses are shown in the figure, the primary and reflected (see also Fig. 3). Each of these excites Ps atoms and causes a momentary increase in the annihilation rate, but for many of our measurements the two laser pulses were almost simultaneous. In either case, however, we observed that after the laser-induced increase in the annihilation rate the total amount of Ps remaining was reduced, evidenced by the slightly lower value of $V(t)$ at later times compared to that obtained without the laser. We note that when the reflected pulse was delayed the returning beam diameter was almost three times larger and covered a greater area of the Ps cloud.

In order to quantify the increased annihilation rate, lifetime spectra with and without laser interactions were compared and difference curves obtained, as shown in Fig. 8. The area of the peaks in the difference curves was taken to represent the number of Ps atoms excited by the laser. Note that neighboring data points are not completely statistically independent due to the 15-ns decay time of the PbWO_4 scintillator. When the primary and reflected laser pulses overlapped [as in Fig. 8(a)], the region just in front of the peak

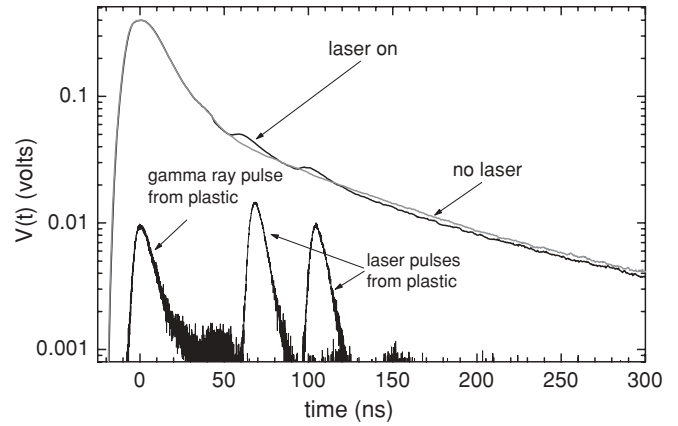


FIG. 7. Single-shot lifetime spectra with and without resonant light interacting with vacuum Ps. The laser pulses shown were detected using a plastic scintillator into which the light was deflected; the primary and reflected light pulses were both measured separately and neither could be measured simultaneously with the lifetime spectra. These data are intended to indicate the relative arrival times of the pulses. For most of the linewidth measurements the second laser pulse was delayed by less than 1 ns, forming in effect a single pulse. Note that the laser pulse width was actually ~ 7 ns wide (FWHM) and not almost 10 ns as implied by Fig. 7. This was due to a long cable partly integrating the detector signal recorded by the oscilloscope. The lifetime spectra are averages of 10 individual shots.

position (70–90 ns) was used as the background for integrating the peak [45]. When the two laser pulses were temporally separated [as in Fig. 8(b)], the region from 150–170 ns was used as the background for integrating the second peak. For

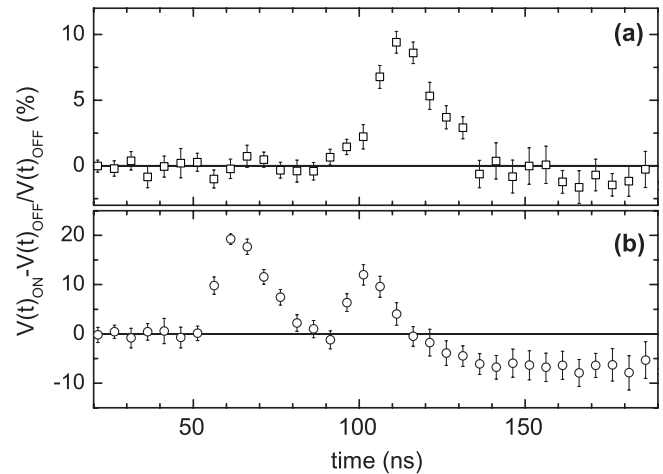


FIG. 8. Single-shot lifetime difference curves obtained with one overlapping resonant laser pulse (a) and both incident and reflected resonant laser pulses, the latter having been delayed by ~ 40 ns by virtue of an extended path length (b). Data of this type were used to obtain the magnitude of the Ps excitation signal. In both cases the long time signal after the laser pulse is negative, indicating that the total amount of Ps remaining after irradiation is less than would have been the case without any laser interactions. The original data have been summed into 5-ns bins, and the error flags represent the standard deviations of the mean of ten measurements. Neighboring data points are correlated due to the 15-ns decay time of the scintillator.

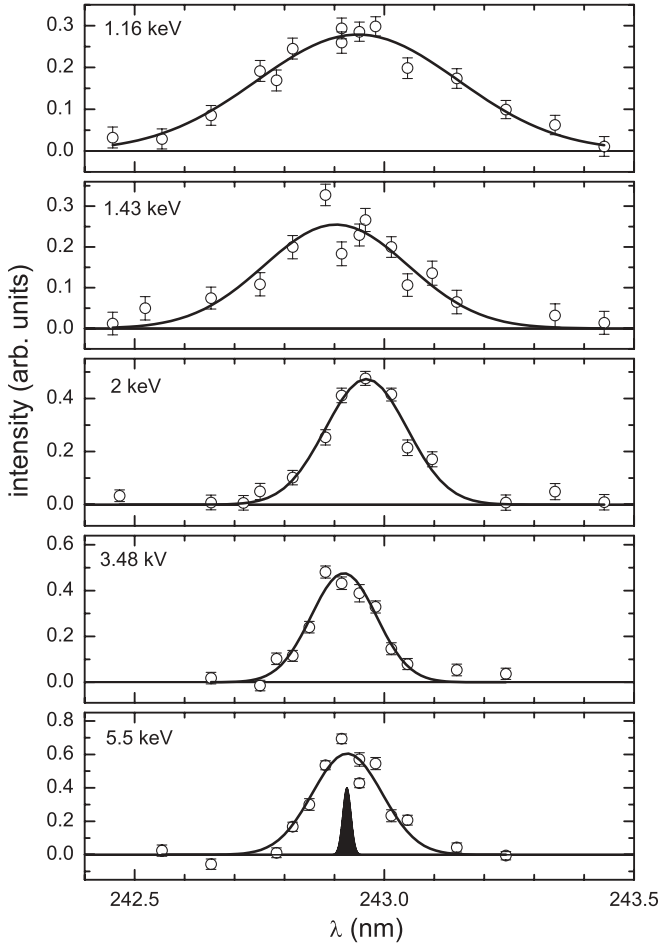


FIG. 9. Linewidth of the 1^3S - 2^3P excitation of positronium created in porous silica for different incident positron beam energies. The solid lines are Gaussian fits constrained to have zero vertical offset, which is guaranteed to be appropriate by the procedure by which the data are analyzed. The variation in the line centers is due to alignment errors in the laser calibration (see text). The 100-GHz FWHM (0.02 nm) probe laser bandwidth is represented by the solid Gaussian curve in the bottom panel. The laser wavelengths are measured in air.

the “single-pulse” measurements the laser power was fixed at $100 \mu\text{J}/\text{pulse}$, while for the separated pulse measurements the power was increased to $\sim 250 \mu\text{J}/\text{pulse}$.

The Doppler-broadened linewidth of the 1^3S - 2^3P transition of positronium was measured from spectra obtained by plotting the areas of the difference curves as a function of the laser wavelength. At each wavelength the mean and standard deviation of the mean of the signal amplitude was determined by averaging over a set of ten shots. The average laser power was measured for each frequency at a repetition rate of 20 Hz, and the data were normalized accordingly. A selection of lines measured in this way is shown in Fig. 9. The lines were fitted using a Gaussian distribution of Doppler-shifted resonant wavelengths,

$$P(\lambda) \propto \exp\left\{-\frac{(\lambda - \lambda_0)^2 c^2}{2\lambda_0^2 \langle v_x^2 \rangle}\right\}, \quad (6)$$

where $\lambda_0 \approx 243 \text{ nm}$ is the resonant wavelength of the 1^3S - 2^3P transition in the rest frame and $\langle v_x^2 \rangle$ is the mean square velocity

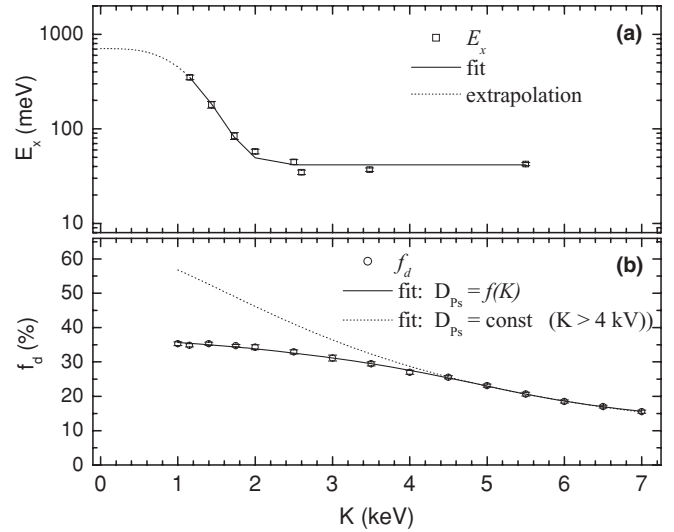


FIG. 10. Mean kinetic energy associated with motion in the x direction, E_x , of Ps emitted into vacuum (a) and the delayed fraction f_d (b) as a function of the incident positron beam energy K . The solid lines are fits to the data as described in the text. The dotted line in (a) is an extrapolation of the fitted curve to illustrate the Ps temperature predicted by Eq. (13) at low energies. The dotted line in (b) is a fit of the standard theory for thermal positronium emission [Eq. (20), see text] to the data for $E > 4 \text{ keV}$ that has been extrapolated back to low energy.

in the x direction. The Doppler line shape FWHM, $\Delta\lambda$, divided by the resonant wavelength, λ_0 , is

$$\frac{\Delta\lambda}{\lambda_0} \approx 2\sqrt{2 \ln 2} \sqrt{\frac{\langle v_x^2 \rangle}{c^2}}. \quad (7)$$

Analyzing the data of Fig. 9 in this way yields the mean positronium kinetic energy $E_x \equiv \frac{1}{2} m_{Ps} \langle v_x^2 \rangle$ associated with motion parallel to the sample surface along the axis of the laser beam, shown in Fig. 10(a) as a function of the positron implantation energy.

In order to check whether or not there might be differences between measurements made at different times with respect to the Ps formation, linewidths were also measured using two laser pulses separated in time, as shown in Fig. 7. Two pairs of linewidths were measured at beam energies of 1.6 and 4.5 keV, shown in Figs. 11(a) and 11(b), respectively [46]. We obtained the same FWHM (within uncertainties) for the 4.5-keV case, with $(0.143 \pm 0.010) \text{ nm}$ for the primary beam and $(0.164 \pm 0.013) \text{ nm}$ for the secondary beam. The low-energy case exhibited a 1.5 standard deviation difference between the two, with FWHM equal to $(0.206 \pm 0.018) \text{ nm}$ for the primary pulse and $(0.281 \pm 0.029) \text{ nm}$ for the secondary pulse. The line centers match exactly within errors. For the 1.6-keV measurements we obtained wavelengths in air of $(242.924 \pm 0.011) \text{ nm}$ and $(242.924 \pm 0.013) \text{ nm}$ for the primary and secondary pulses, respectively, and for the 4.5-keV case we measured $(242.946 \pm 0.008) \text{ nm}$ and $(242.940 \pm 0.009) \text{ nm}$ for the primary and secondary pulses, respectively. One might have expected that faster atoms should be detected first and that we should have observed an increased linewidth using the primary (earlier) laser pulse. The fact that we observe no

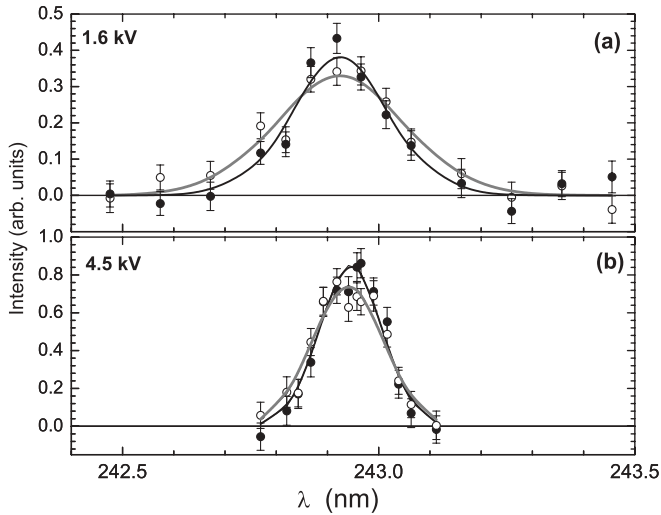


FIG. 11. Line shapes taken using double-laser pulses for positron beam energies of 1.6 kV (a) and 4.5 kV (b). In both panels the primary laser beam data are represented by the solid circles, with fitted curves in black, and the reflected beam data are represented by the open circles, with grey fitted curves.

evidence for this probably means that the effective volume in front of the target covered by the laser was larger than might be expected from the observed beamwidth of ~ 6 mm, due to the high degree of saturation of the transition, making it possible to excite Ps atoms efficiently far out in the wings of the beam profile. This would also explain why we are able to detect both fast and slow Ps with similar efficiencies.

Our 12 measured line centers yield an unweighted mean and standard deviation of the distribution (corrected for the refractive index of air $n = 1.00027$) of (242.998 ± 0.016) nm, 1.4 standard deviations less than the vacuum wavelength 243.021 nm of the 1^3S_1 - 2^3S_1 interval measured by Chu, Mills, and Hall [47].

IV. DISCUSSION

A. Measurements

Although Ps has been routinely produced experimentally for decades [3,48] and can easily be produced at thermal temperatures in ultra-high vacuum conditions using slow positron beams [49] there have been few experiments involving Ps laser spectroscopy [50]. This is largely because positronium atoms are in general produced at low intensities and the resulting signal is therefore very weak. Nevertheless, high-precision measurements of the 1^3S_1 - 2^3S_1 transition of Ps have been carried out by Chu *et al.* [47,51,52]. This transition was observed via a two-photon excitation and was therefore Doppler free (to first order). The optical saturation of the 1^3S_1 - 2^3P_J transition [53] as well as the production of high n states [54] of Ps were observed by Ziock *et al.* using a broadband laser.

The relatively small change in the Ps lifetime spectra caused by laser excitation (see Figs. 7 and 8) is mostly because of the very large Doppler-broadened linewidth of the transition. This is an inevitable result when dealing with Ps which is orders of magnitude lighter than other atoms. The maximum (resonant)

absorption cross section for a two-level atom with absorption wavelength λ_0 is [55]

$$\sigma(\lambda_0) = \frac{3\lambda_0^2}{2\pi}. \quad (8)$$

For the $1S$ - $2P$ transition in positronium this wavelength is 243 nm, which gives a resonant cross section of $\sim 3 \times 10^{-10}$ cm². We can estimate the laser intensity I_{sat} required to saturate this transition from the simple steady-state case using [55]

$$I_{\text{sat}} = \frac{\pi \hbar c}{3\lambda_0^3 \tau_{2P}}, \quad (9)$$

where τ_{2P} is the lifetime of the $2P$ state (3.2 ns). This gives $I_{\text{sat}} \sim 0.5$ W/cm², or approximately 3.5 nJ *per linewidth* for a 1-cm² 7-ns wide pulse. The natural $1S$ - $2P$ linewidth is $1/2\pi \tau_{2P} = 50$ MHz, so that the energy per pulse needed to saturate the transition is $\sim (\Gamma_{\text{laser}}/50 \text{ MHz}) \times 3.5 \text{ cm}^{-2} = 2000 \times 3.5 \text{ nJ cm}^{-2} = 7 \mu\text{J cm}^{-2}$ for our broadband 243-nm laser pulses with $\Gamma_{\text{laser}} = 100$ GHz (see Fig. 9). The amplitude of the observed signal increased by around 50% when the power was increased from 100 to 200 μJ (with an ~ 6 -mm beam diameter), which is much more than the aforementioned estimate of I_{sat} . Our signal is, however, consistent with the measurements and Monte-Carlo simulations of Ziock *et al.* [53] who found that their signal did not approach saturation until the laser power was increased to more than 200 $\mu\text{J cm}^{-2}$. The actual dependence of the signal on the laser power will depend on the details of the spatial and frequency characteristics of the laser as well as on the dynamics of the excitation and annihilation processes [40].

Of all the Ps atoms irradiated by the laser we would expect $<10\%$ to be in resonance (since the laser width is $<10\%$ of the Doppler-broadened linewidth). Also, only triplet $2P$ states that mix with the singlet states will be detected, which cuts the signal down by another factor of 10 [see Eq. (5)]. Moreover, if there is an electric field in the direction of the magnetic field (which could occur due to charging of the sample substrate) then some $2P$ states could be Stark shifted into $2S$ states, which are long-lived and therefore not detected [40]. We could, however, observe all $2P$ atoms by photo-ionizing them with approximately 100 mJ/cm² of 532-nm light [52], which will be done in future work. This method will also be necessary if one wishes to observe Ps in a magnetic-field-free region, as may be required in similar experiments to observe molecular positronium [17,56].

B. Ps cooling

The cooling of Ps in gases, powders, and porous materials has been studied for many years using a variety of experimental methods [57–62]. A model developed by Nagashima and co-workers to describe Ps energy loss by collisions (with gas atoms or grains in powders) has been able to successfully describe Ps cooling rates in materials with mean free paths ranging from 5 to 70 nm [63]. This model is classical and describes ground-state Ps atoms losing energy through repeated collisions with heavier particles. While this may be an appropriate description for systems involving what are in effect free particles colliding with large grains or gas molecules, it

may not apply in the case of Ps confined to small pores. Indeed, if the Ps de Broglie wavelength at kinetic energy E_{Ps} ,

$$\lambda_{Ps} = h(2m_{Ps}E_{Ps})^{-1/2} \sim 0.9 \text{ nm}(1 \text{ eV}/E_{Ps})^{1/2}, \quad (10)$$

is close to the size of the pores, then a classical model may not properly describe Ps cooling or diffusion as they will be dominated by quantum effects. In particular, the energy levels of Ps in the pore must be taken into account, diffusion between interconnected pores may proceed predominantly through tunneling processes, and energy transfer to the surrounding material will depend on the overlap of the Ps wave function with the internal pore surfaces and any atoms or molecules that may reside thereon [62].

Ps is emitted from the bulk material into the pores with an energy of at least 1 eV, and possibly as much as 3 eV. Nagashima *et al.* [64] have attributed peaks observed at 1 and 3 eV to bulk and surface emission, respectively. In fact, various emission energies have been observed, all in the range of 1–3 eV [65–68]. The exact value in a given sample may depend on surface chemistry or bulk impurities. We can say that the Ps emission energy will be at least 1 eV, which means that upon emission the de Broglie wavelength is less than 1 nm, while the pore diameter is almost three times larger, and so initially a classical approximation may be adequate. However, as the Ps cools and the wavelength becomes comparable to the pore size this is no longer the case. We have then a slightly unusual system that starts off in a classical regime and ends up being entirely quantum mechanical in nature. The cooling process happens fairly quickly [see Eq. (23)] and essentially stops when the Ps wavelength is close to the pore size. Conversely, the motion of Ps that is not implanted near the surface occurs mostly after the cooling has stopped. This means that we can, broadly, consider the cooling to be a classical process and the diffusion of cooled Ps to be a quantum process.

We assume, just as in the classical model, that Ps atoms of total energy E_{Ps} lose energy via interactions with a surface [63,69] such that after each interaction the energy changes by

$$\Delta E = -\alpha(E_{Ps} - E_{\min}). \quad (11)$$

Here E_{\min} is the minimum mean total energy of a thermalized Ps atom in a pore, and α is the fractional energy loss per interaction, $\sim 8 \times 10^{-5}$ based on the relative mass of Ps and the atomic constituents of SiO_2 [69]. After N interactions the mean Ps energy will be

$$E_{Ps} = E_i \exp\{-\alpha N\} + E_{\min}, \quad (12)$$

where E_i is the initial energy with which the Ps was emitted from the bulk material, and we have assumed that $E_i \gg E_{\min}$. The Ps is formed by implanting positrons at a kinetic energy K into the target, which results in a mean implantation depth given by [70]

$$\bar{x} = \frac{A}{\rho} K^{\nu}. \quad (13)$$

Here K is in keV, $\nu \approx 1.7$, $A = 2.81 \mu\text{g}/\text{cm}^2$ [71], and $\rho = 1.35 \text{ g}/\text{cm}^3$ is the average target material density.

For a classical particle bouncing off the pore walls we would assume that the Ps atoms diffuse toward the surface with a velocity-independent mean free path Λ , such that the average

number of collisions upon reaching the surface is

$$N = 3(\bar{x}/\Lambda)^2 C^2 = \frac{3A^2 K^{2\nu} C^2}{\rho^2 \Lambda^2}. \quad (14)$$

Here C is the mean number of collisions that take place in each pore. The mean free path in this case is the pore spacing, Λ (see Fig. 4). The final energy E_{Ps} of the Ps after reaching the surface, in terms of the positron implantation energy K , will be given by

$$\begin{aligned} E_{Ps}(K) &= E_i \exp\{-3\alpha A^2 K^{2\nu} C^2 / \rho^2 \Lambda^2\} + E_{\min} \\ &\equiv E_i \exp\{-QK^{2\nu}\} + E_{\min}. \end{aligned} \quad (15)$$

In fitting Eq. (15) to the data shown in Fig. 10(a) we must remember that the total Ps kinetic energy of Eq. (15) includes components associated with motion in all directions. We therefore multiply the data of Fig. 10(a) by some factor η to account for the fact that the measurements are made in only one direction. The fit then yields $E_i = \eta(0.65 \pm 0.03) \text{ eV}$, $Q = 0.49 \pm 0.03$, and $E_{\min} = \eta(41.7 \pm 2.7) \text{ meV}$. The value of E_i is consistent with the emission energies observed in other experiments for η in the range of 1.5–4.6 [64,66–68]. We return to the discussion of E_{\min} later in this article. The measured value of Q implies that the mean number of collisions per pore is $C = 7$. This in turn implies that b , the diameter of the hole between pores, is $\sim 0.6 \text{ nm}$ (see Sec. II B). For a channel diameter of this size we would therefore expect that diffusion will proceed primarily via tunneling for Ps energies below around $\sim 3 \text{ eV}$, which would mean that this is the only way for Ps atoms to move around in a sample such as that used here. This reiterates the quantum nature of this system and the need for caution when employing a classical approximation.

The cooling of Ps in porous films and subsequent emission into vacuum has been studied several times before via Ps time-of-flight (TOF) measurements [66,67]. Similar behavior of the Ps energy as a function of the implantation beam energy has been observed, including one measurement made with a sample identical to that used in this work, in which a minimal energy above thermal levels was also seen [72]. Yu *et al.* [66] observed the same qualitative Ps energy dependence on beam energy for two different samples, but found that the sample with the largest pore sizes gave the hottest Ps energy at high implantation energy, which is not in accord with our model of Ps confinement. However, a second sample with slightly smaller pore sizes exhibited essentially the same energy dependence, with a lower limit of $\sim 70 \text{ meV}$ for 4-keV incident positrons. This was attributed to different cooling rates due to different pore structures, although the form of the data looks very much like our observations.

Ito *et al.* [67] observed Ps cooling in one sample to near thermal energy (50 meV) but the data are not sufficiently unambiguous to distinguish between incomplete thermalization and a lower “temperature” limit due to confinement. The pores were estimated to be approximately 2.2 nm in diameter, although this estimate is model dependent and the actual pore size could well be significantly larger. Tanaka *et al.* [73] observed similar results and attributed the form of the Ps cooling to a bimodal pore structure resulting in an energy-dependent tortuosity [74], and hence cooling. However, we believe that this is incorrect since identical cooling has been

observed in films that are not expected to have bimodal pore structures.

C. Ps confinement energy

As Ps cools by collisions in porous media the interaction rate with the walls decreases, and thus the cooling rate must also decrease, which can lead to incomplete thermalization [63]. However, even under these circumstances the measured temperature of emitted Ps would still be expected to decrease as the implantation depth is increased because only Ps that was able to escape into vacuum was excited by the laser; Ps atoms that were trapped in the sample were not part of the signal. As the implantation energy is increased, atoms that are able to escape, while fewer in number, must necessarily interact with the walls as they diffuse to the surface, and hence should continue to cool down to thermal temperatures. However, the data unambiguously indicate that rather than continuing to cool to thermal levels the Ps energy relaxed to a constant value that was significantly higher than we would expect from a room-temperature sample. We suggest that, since the energy difference between the ground and the first excited state of Ps confined in the pores is much greater than kT , the minimum Ps energy is simply its confinement energy.

The lowest energy state of a Ps atom confined in an idealized spherical pore of radius a and diameter $d = 2a$ is

$$E_0 = \frac{\pi^2 \hbar^2}{2m_{\text{Ps}} a^2} = 753 \text{ meV} (1 \text{ nm}/d)^2. \quad (16)$$

For an effective pore diameter of 2.4 nm (taking into account the fact that the Ps center of mass can get no closer to the wall than a mean *radius* ~ 0.16 nm) [13,75], $E_0 = 131$ meV. Thus, the Ps is emitted into vacuum with a kinetic energy E_{min} equal to E_0 . Note that E_{min} has no significant thermal component because the excited states are largely inaccessible at room temperature.

In order to properly compare the confinement energy E_0 with the value of $E_{\text{min}} = \eta(41.7 \pm 2.7)$ meV obtained from the fit to Fig. 10(a) we need to know something about the parameter η . If we were simply considering a thermal Maxwell-Boltzmann distribution we would expect the energy to be distributed equally in all directions, and therefore also $\eta = 3$. However, in the present case there is no thermal distribution, and we have monoenergetic Ps (with velocity v_0) that is emitted from the surface by randomly orientated pores. We assume that this emission occurs with an angular distribution proportional to $\cos\theta$, where θ is the angle of emission relative to the normal to the surface which is the v_z axis. The projection of this distribution onto the v_x - v_y plane is a constant density. The projection of this in turn onto the v_x axis is proportional to $\sqrt{v_0^2 - v_x^2}$ for $v_x^2 < v_0^2$ and zero otherwise. The mean square value of v_x is then

$$\langle v_x^2 \rangle = \int_0^{v_0} v_x^2 \sqrt{v_0^2 - v_x^2} dv_x \bigg/ \int_0^{v_0} \sqrt{v_0^2 - v_x^2} dv_x = \frac{1}{4} v_0^2, \quad (17)$$

that is, $\eta = 4$. Our data seem to imply that $\eta \sim 3$, which could mean that the angular distribution differs from $\cos\theta$, or that the pore diameter is $\sim 10\%$ smaller than expected.

D. Ps diffusion

The amount of Ps that manages to diffuse to the sample surface and escape into the vacuum is shown in Fig. 10(b). Positron diffusion in bulk materials has been extensively studied for many years [76]. Usually one considers thermalized positrons diffusing to a surface (with a constant diffusion coefficient) where they may form positronium. The present situation is rather different from the usual case of diffusion in that the Ps diffusion coefficient is changing as E_{Ps} decreases with time, precluding a precise closed-form expression with which to describe the data in Fig. 10(b). We obtain a simple expression for the positronium yield as a function of implantation energy K by assuming that the diffusion coefficient is simply a function of the emitted Ps kinetic energy E_{Ps} :

$$D_{\text{Ps}} = D_{\text{Ps}}(E_{\text{Ps}}) = \frac{\Lambda}{3C} \sqrt{2E_{\text{Ps}}/m_{\text{Ps}}}. \quad (18)$$

The triplet Ps yield is then [77]

$$f_d = \frac{f_0}{1 + \bar{x}/\sqrt{D_{\text{Ps}}\tau}}. \quad (19)$$

At high implantation energies where D_{Ps} has become constant, this expression is equivalent to the familiar expression [70,76,78]

$$f_d = \frac{f_0}{1 + (K/K_0)^v}, \quad (20)$$

where K_0 is the implantation energy at which half of the positronium is able to diffuse to the surface (the ‘‘half energy’’) [44]. Here f_0 is the branching ratio for Ps formation at the surface (modified to reflect the fact that f_d is not the exact Ps fraction). For lower positron impact energies, Eq. (20) does not fit the data very well, primarily because the Ps is then not thermalized and E_{Ps} and the diffusion coefficient both depend on K as in Eqs. (15) and (18).

Combining Eqs. (13), (15), (18), and (19) we obtain

$$f_d = \frac{f_0}{1 + K^v A_1^{-1} (E_i \exp\{-QK^{2v}\} + E_{\text{min}})^{-1/4}}. \quad (21)$$

Equation (21) fits the data of Fig. 10(b) quite well. At low positron implantation energies (i.e., for $K < \sim 2$ kV) the energetic Ps diffuses rapidly so that the emitted fraction f_d hardly changes at all until the Ps energy falls below around 50 mV. For Ps at a constant energy (i.e., for $K > \sim 2$ kV), the diffusion coefficient D_{Ps} does not change significantly with implantation depth and the emission characteristics are very similar to those ordinarily observed for positron diffusion. For comparison we also show in this figure a fit of the same data for $K > 4$ kV to Eq. (20). At higher energies (where we expect the diffusion coefficient to be constant) the two fitted curves are identical, but for hotter Ps, where this is not the case, they diverge.

When $K = K_0$ the implantation depth is approximately equal to the mean diffusion length $L \equiv \bar{x}(K_0)$, so that [cf. Eq. (13)]

$$L = \frac{A}{\rho} K_0^v = \sqrt{2D_{\text{Ps}}\tau_L}, \quad (22)$$

where $\tau_L = \tau/2$ is the mean time for Ps to reach the surface from a depth L . The Ps lifetime in the pores was directly

measured using a sample identical to that used in this work apart from a capping layer [42]. The measured value of $\tau = 50$ ns is consistent with the 2.7-nm pore size [13] as well as our measurements. Using $\tau_L = 25$ ns and $K_0 \sim 6$ kV [see Fig. 10(b)] we find from Eq. (22) $D_{\text{Ps}} = 0.038$ cm²/s. Then we may estimate the mean time for Ps emission as a function of implantation energy. For energies greater than 2 keV, such that the Ps has thermalized in the pores, we find

$$t = \bar{x}^2/2D_{\text{Ps}} = \frac{A^2}{2D_{\text{Ps}}\rho^2} K^{2v} = 57 \text{ ps} K^{2v}. \quad (23)$$

For energies less than 2 keV, such that the Ps has not thermalized in the pores, the emission times will be about 100 times shorter. It should therefore be possible to produce thermalized short-lived positronic objects in a porous target such that the products (singlet Ps, Ps⁺, Ps⁻, Ps₂, or even other Ps or positron-atom compounds [79,80]), can escape into vacuum for spectroscopic experiments before annihilating.

V. CONCLUDING REMARKS

To summarize, when positrons are implanted into porous silica films positronium may be created which is subsequently able to escape into the vacuum if the pores are interconnected and the film is not capped. The amount and temperature of such positronium depends on the incident beam energy, since deeper implantation means more collisions before emission.

We have measured the energy of Ps emitted from such a film (in one dimension) using Doppler spectroscopy of intense bunches of Ps atoms. This methodology also demonstrates that we can generate bunches containing large numbers of excited-state atoms, which will be necessary for Ps laser cooling as well as experiments involving Ps₂ and antihydrogen. For the production of cold Ps in the manner described here our data indicate that a porous sample would need to be composed of pores with a diameter greater than 10 nm in order to produce Ps in vacuum with effective temperatures less than 100 K [81].

Applying a simple model we have been able to describe the Ps emission temperature and fraction with surprising efficacy. The model describes Ps cooling via interactions of confined Ps with the surrounding medium and explains the emission of hot Ps via a temperature-dependent diffusion coefficient. This model is a crude approximation, however, and a full quantum mechanical treatment is required to properly describe the regime in which Ps is confined in a system

whose dimensions are of the same order as the Ps de Broglie wavelength [82]. A lower limit to the Ps emission energy was observed that is consistent with the conversion of the ground-state energy of Ps confined in the pores to kinetic energy following emission into vacuum. Using films with an ordered pore structure this mechanism could provide a method for producing almost monoenergetic Ps in vacuum, which may be useful for spectroscopy and scattering experiments [83].

In future work we will measure the laser power transmitted through the target chamber on a shot by shot basis so as to know the applied power exactly. We also plan to stabilize the laser room temperature and include continuous measurements of the laser frequency so that we can measure absolute values for line centers. In the present case this was not very important as the Ps Lyman α frequency is very well known, but we also intend to measure the energy intervals to the Ps₂ excited states [84,85]. Knowledge of these frequencies can be compared directly to calculations and it should be possible to measure them to a precision of ~ 10 ppm. Clearly for these measurements we will need to know the absolute laser frequency as accurately as possible.

TOF measurements using a sample identical to that used here as well as one with larger pore size are in agreement with the present work [72,86]; it was found that Ps was emitted with a minimal energy above $kT/2$ whose value decreased when a larger pore size was used. Detailed studies of the Ps temperature for high-impact energies using a range of different pore sizes should help to elucidate the mechanisms leading to the conversion of the zero point energy to free Ps kinetic energy and also to establish whether or not this might be used as a “tunable” source of cold Ps. Such experiments would also help to understand Ps cooling in more complex structures designed to achieve very-low-temperature Ps for the production of a Ps Bose-Einstein condensate (BEC) [18]. For example, Ps cooling has been observed down to ~ 50 K [87] and understanding the limiting factors in this process could help to mitigate the demanding Ps density requirements.

ACKNOWLEDGMENTS

The authors gratefully acknowledge the work of C. Corbel, M.-F. Barthe, and U. Gendotti for the sample selection. This work was supported in part by the National Science Foundation under Grants PHY 0537431, PHY 0555701, and PHY 0900919.

-
- [1] For a review of Ps properties, see A. Rich, *Rev. Mod. Phys.* **53**, 127 (1981).
 [2] For a review of positron interactions with surfaces, see P. J. Schultz and K. G. Lynn, *Rev. Mod. Phys.* **60**, 701 (1988).
 [3] K. F. Canter, A. P. Mills Jr., and S. Berko, *Phys. Rev. Lett.* **33**, 7 (1974).
 [4] A. P. Mills Jr., *Phys. Rev. Lett.* **41**, 1828 (1978).

- [5] J. Callaway, *Phys. Rev.* **116**, 1140 (1959).
 [6] R. E. Bell and R. L. Graham, *Phys. Rev.* **90**, 644 (1953).
 [7] P. Sferlazzo, S. Berko, and K. F. Canter, *Phys. Rev. B* **32**, 6067 (1985).
 [8] D. W. Gidley, H.-G. Peng, and R. S. Vallery, *Annu. Rev. Mater. Res.* **36**, 49 (2006).
 [9] C. Jin, J. D. Luttmer, D. M. Smith, and T. A. Ramos, *MRS Bull.* **22**, 39 (1997).

- [10] E.g., G. Frenzer and W. F. Maier, *Annu. Rev. Mater. Res.* **36**, 281 (2006).
- [11] S. J. Tao, *J. Chem. Phys.* **56**, 5499 (1972).
- [12] M. Eldrup, D. Lighbody, and J. N. Sherwood, *Chem. Phys.* **63**, 51 (1981).
- [13] D. W. Gidley, W. E. Frieze, T. L. Dull, A. F. Yee, E. T. Ryan, and H.-M. Ho, *Phys. Rev. B* **60**, R5157 (1999).
- [14] E.g., C. J. Brinker and G. W. Scherer, *The Physics and Chemistry of Sol-Gel Processing* (Academic Press, New York, 1990).
- [15] D. B. Cassidy, S. H. M. Deng, R. G. Greaves, T. Maruo, N. Nishiyama, J. B. Snyder, H. K. M. Tanaka, and A. P. Mills, *Phys. Rev. Lett.* **95**, 195006 (2005).
- [16] D. B. Cassidy and A. P. Mills Jr., *Phys. Rev. Lett.* **100**, 013401 (2008).
- [17] D. B. Cassidy and A. P. Mills Jr., *Nature (London)* **449**, 195 (2007).
- [18] P. M. Platzman and A. P. Mills Jr., *Phys. Rev. B* **49**, 454 (1994).
- [19] M. Amoretti *et al.*, *Nature (London)* **419**, 456 (2002).
- [20] J. W. Humberston, M. Charlton, F. M. Jacobsen, and B. I. Deutch, *J. Phys. B* **20**, L25 (1987).
- [21] M. Charlton, *Phys. Lett.* **A143**, 143 (1990).
- [22] D. B. Cassidy, J. P. Merrison, M. Charlton, J. Mitroy, and G. Ryzhikh, *J. Phys. B* **32**, 1923 (1999).
- [23] P. Perez and A. Rosowsky, *Nucl. Instrum. Methods Phys. Res. A* **532**, 523 (2004).
- [24] A. Kellerbauer *et al.*, *Nucl. Instrum. Methods Phys. Res. Sec. B* **266**, 351 (2008).
- [25] F. Castelli, I. Boscolo, S. Cialdi, M. G. Giammarchi, and D. Comparat, *Phys. Rev. A* **78**, 052512 (2008).
- [26] D. B. Cassidy, S. H. M. Deng, R. G. Greaves, and A. P. Mills, Jr., *Rev. Sci. Instrum.* **77**, 073106 (2006).
- [27] C. M. Surko and R. G. Greaves, *Phys. Plasmas* **11**, 2333 (2004).
- [28] F. Anderegg, E. M. Hollmann, and C. F. Driscoll, *Phys. Rev. Lett.* **81**, 4875 (1998).
- [29] R. G. Greaves and C. M. Surko, *Phys. Rev. Lett.* **85**, 1883 (2000).
- [30] A. P. Mills Jr., *Appl. Phys.* **23**, 189 (1980).
- [31] D. B. Cassidy, S. H. M. Deng, H. K. M. Tanaka, and A. P. Mills Jr., *Appl. Phys. Lett.* **88**, 194105 (2006).
- [32] D. B. Cassidy and A. P. Mills Jr., *Nucl. Instrum. Methods Phys. Res. Sec. A* **580**, 1338 (2007).
- [33] O. Halpern, *Phys. Rev.* **88**, 164 (1952).
- [34] A. Rich, Ph.D. dissertation, University of Michigan, 1965 (available from UMI Dissertation Services, Ann Arbor, MI), p. 80.
- [35] R. M. Drisko, *Phys. Rev.* **102**, 1542 (1956).
- [36] D. B. Cassidy, K. T. Yokoyama, S. H. M. Deng, D. L. Griscom, H. Miyadera, H. W. K. Tom, C. M. Varma, and A. P. Mills Jr., *Phys. Rev. B* **75**, 085415 (2007).
- [37] H. Saito and T. Hyodo, *Phys. Rev. B* **60**, 11070 (1999).
- [38] S. M. Curry, *Phys. Rev. A* **7**, 447 (1973).
- [39] M. L. Lewis and V. W. Hughes, *Phys. Rev. A* **8**, 625 (1973).
- [40] C. D. Dermer and J. C. Weisheit, *Phys. Rev. A* **40**, 5526 (1989).
- [41] Y. Cohen, K. Landskron, N. Tetreault, S. Fournier-Bidoz, B. Hatton, and G. A. Ozin, *Adv. Funct. Mater.* **15**, 593 (2005).
- [42] L. Liskay, C. Corbel, P. Perez, P. Desgardin, M.-F. Barthe, T. Ohdaira, R. Suzuki, P. Crivelli, U. Gendotti, A. Rubbia, M. Etienne, and A. Walcarius, *Appl. Phys. Lett.* **92**, 063114 (2008).
- [43] Here we have neglected the volume occupied by the interconnecting channels. Since the maximum density for a HCP structure with no spaces between spheres is $\rho/\rho_0 = 0.74$ [J. Kepler, *Strena seu de nive sexangula* (1611), edited and translated by Colin Hardie (Clarendon Press, Oxford, 1966).], this will lead to an underestimate of Λ of less than 10%.
- [44] The BBO crystal used was $6 \times 6 \times 10$ mm, was AR coated for 355 nm and 760–800 nm, and was cut at an angle of 52.1° . The crystal was mounted in a cell with a Brewster window at the input and an AR-coated fused silica window at the output. The cell had a static seal with helium gas and the crystal was mounted on an adjustable platform to adjust the z and x axis. The y axis, which optimizes the phase-matching angle, was rotated using a commercial motorized rotational stage. The rotation along the y axis was used to produce sum frequency mixing of 243 nm light at 49.8° .
- [45] The number of counts in the background region differed from zero (by $<5\%$, see Fig. 7) because of small drifts associated with changes in the Ps fraction due to charging of the glass sample substrate. Since the form of the laser-off lifetime spectra is independent of the beam energy in the background region, the background determined in this way properly accounts for small changes in the Ps fraction between the laser-on and laser-off measurements.
- [46] The data shown in Fig. 10 have statistics poorer than those found in Fig. 8 because of larger than usual variations in the power applied to the interaction region caused by a less than optimal mode structure.
- [47] S. Chu, A. P. Mills, and J. L. Hall, *Phys. Rev. Lett.* **52**, 1689 (1984).
- [48] M. Deutsch, *Phys. Rev.* **82**, 455 (1951).
- [49] A. P. Mills and L. Pfeiffer, *Phys. Rev. Lett.* **43**, 1961 (1979).
- [50] An early attempt to observe Ps excitation using a lamp did show a small fraction of $n = 2$ Ps. S. L. Varghese, E. S. Ensberg, V. W. Hughes, and I. Lindgren, *Phys. Lett.* **A49**, 415 (1974).
- [51] S. Chu and A. P. Mills, *Phys. Rev. Lett.* **48**, 1333 (1982).
- [52] M. S. Fee, A. P. Mills, S. Chu, E. D. Shaw, K. Danzmann, R. J. Chichester, and D. M. Zuckerman, *Phys. Rev. Lett.* **70**, 1397 (1993).
- [53] K. P. Ziock, C. D. Dermer, R. H. Howell, F. Magnota, and K. M. Jones, *J. Phys. B* **23**, 329 (1990).
- [54] K. P. Ziock, R. H. Howell, F. Magnotta, R. A. Failor, and K. M. Jones, *Phys. Rev. Lett.* **64**, 2366 (1990).
- [55] E.g., C. J. Foot, *Atomic Physics* (Clarendon Press, Oxford, 2005).
- [56] D. B. Cassidy *et al.*, *J. Phys.: Conf. Ser.* **194**, 012037 (2009).
- [57] T. Chang, M. Xu, and X. Zeng, *Phys. Lett.* **A126**, 189 (1987).
- [58] A. P. Mills, E. D. Shaw, R. J. Chichester, and D. M. Zuckerman, *Phys. Rev. B* **40**, 2045 (1989).
- [59] Y. Nagashima, M. Kakimoto, T. Hyodo, K. Fujiwara, A. Ichimura, T. Chang, J. Deng, T. Akahane, T. Chiba, K. Suzuki, B. T. A. McKee, and A. T. Stewart, *Phys. Rev. A* **52**, 258 (1995).
- [60] C. Dauwe, B. Waeyenberge, D. Segers, T. Hoecke, and J. Kuriplach, *J. Radiol. Nucl. Chem.* **210**, 293 (1996).
- [61] Y. Nagashima *et al.*, *J. Phys. B* **31**, 329 (1998).
- [62] C. He, T. Ohdaira, N. Oshima, M. Muramatsu, A. Kinomura, R. Suzuki, T. Oka, and Y. Kobayashi, *Phys. Rev. B* **75**, 195404 (2007).
- [63] H. Saito and T. Hyodo, in *New Directions in Antimatter Chemistry and Physics*, edited by C. M. Surko and F. A. Gianturco (Kluwer, Dordrecht, 2001), p. 101.
- [64] Y. Nagashima, Y. Morinaka, T. Kurihara, Y. Nagai, T. Hyodo, T. Shidara, and K. Nakahara, *Phys. Rev. B* **58**, 12676 (1998).

- [65] P. Sferlazzo, S. Berko, and K. F. Canter, *Phys. Rev. B* **35**, 5315 (1987).
- [66] R. S. Yu, T. Ohdaira, R. Suzuki, K. Ito, K. Hirata, K. Sato, Y. Kobayashi, and J. Xu, *Appl. Phys. Lett.* **83**, 4966 (2003).
- [67] K. Ito, R. S. Yu, K. Sato, K. Hirata, Y. Kobayashi, T. Kurihara, M. Egami, H. Arao, A. Nakashima, and M. Komatsu, *J. Appl. Phys.* **98**, 094307 (2005).
- [68] H. K. M. Tanaka, T. Kurihara, and A. P. Mills Jr., *Phys. Rev. B* **72**, 193408 (2005).
- [69] G. W. Ford, L. M. Sander, and T. A. Witten, *Phys. Rev. Lett.* **36**, 1269 (1976).
- [70] A. P. Mills Jr., and R. J. Wilson, *Phys. Rev. A* **26**, 490 (1982).
- [71] J. Algers, P. Sperr, W. Egger, G. Kögel, and F. H. J. Maurer, *Phys. Rev. B* **67**, 125404 (2003).
- [72] U. Gendotti, Ph.D. thesis, unpublished, ETH, Zurich, Switzerland, 2009.
- [73] H. K. M. Tanaka, T. Kurihara, and A. P. Mills, *J. Phys. Condens. Matter* **18**, 8581 (2006).
- [74] E.g., R. W. Mair, G. P. Wong, D. Hoffmann, M. D. Hürlimann, S. Patz, L. M. Schwartz, and R. L. Walsworth, *Phys. Rev. Lett.* **83**, 3324 (1999).
- [75] K. L. Cheng and Y. C. Jean, in *Positron and Positronium Chemistry*, edited by D. M. Schrader and Y. C. Jean (Elsevier, Amsterdam, 1979), p. 282.
- [76] A. P. Mills Jr., in *Positron Solid-State Physics, Proceedings of the International School of Physics, Enrico Fermi, Course LXXXIII*, edited by W. Brandt and A. Dupasquier (North-Holland, Amsterdam, 1981), p. 432. See Eq. (2.3.4).
- [77] Allen P. Mills Jr., and Cherry A. Murray, *Appl. Phys.* **21**, 323 (1980).
- [78] K. G. Lynn and H. Lutz, *Phys. Rev. B* **22**, 4143 (1980).
- [79] D. M. Schrader and J. Moxom, in *New Directions in Antimatter Chemistry and Physics*, edited by C. M. Surko and F. A. Gianturco (Kluwer, Dordrecht, 2001), p. 263.
- [80] J. Mitroy, M. W. J. Bromley, and G. G. Ryzhikh, *J. Phys. B* **35**, R81 (2002).
- [81] See also S. Mariazzi, A. Salemi, and R. S. Brusa, *Phys. Rev. B* **78**, 085428 (2008).
- [82] See also L. Liskay, C. Corbel, L. Raboin, J.-P. Boilot, P. Perez, A. Brunet-Bruneau, P. Crivelli, U. Gendotti, A. Rubbia, and T. Ohdaira, *Appl. Phys. Lett.* **95**, 124103 (2009).
- [83] G. Laricchia, S. Armitage, A. Kover, and D. J. Murtagh, *Advances Atomic, Molecular, and Optical Physics*, edited by E. Arimondo, P. R. Berman, and C. C. Lin (Academic Press, New York, 2008), Vol. 56, pp. 1–47.
- [84] K. Varga, J. Usukura, and Y. Suzuki, *Phys. Rev. Lett.* **80**, 1876 (1998).
- [85] M. Puchalski and A. Czarnecki, *Phys. Rev. Lett.* **101**, 183001 (2008).
- [86] P. Crivelli, U. Gendotti, A. Rubbia, C. Corbel, L. Liskay, and P. Perez (to be published).
- [87] C. G. Fischer, M. H. Weber, C. L. Wang, S. P. McNeil, and K. G. Lynn, *Phys. Rev. B* **71**, 180102(R) (2005).